Journal of Zhejiang University-SCIENCE A (Applied Physics & Engineering)
ISSN 1673-565X (Print); ISSN 1862-1775 (Online)
www.jzus.zju.edu.cn; www.springerlink.com
E-mail: jzus@zju.edu.cn

Radiative energy flux characteristics and model analysis for one-dimensional fixed-bed oxy-coal combustion*

Shi-quan SHAN[†1,2], Zhi-jun ZHOU[†‡1], Zhi-hua WANG[1], Ke-fa CEN[1]

[1]*State Key Laboratory of Clean Energy Utilization, Zhejiang University, Hangzhou 310027, China*

[2]*George W. Woodruff School of Mechanical Engineering, Georgia Institute of Technology, Atlanta, GA 30332, USA*

[†]E-mail: shiquan1204@zju.edu.cn; zhouzj@zju.edu.cn

Received Nov. 22, 2018; Revision accepted May 6, 2019; Crosschecked May 25, 2019

Abstract: This paper describes the radiative energy flux characteristics of fixed-bed oxy-coal combustion for the purpose of guiding the quality-splitting conversion of combustion energy. An experiment was performed in a tube furnace at a temperature range of 800–1200 °C in O_2/N_2 and O_2/CO_2 atmospheres, and the radiative intensity was measured. It was found that an increase in oxygen concentration and temperature could increase the radiative intensity more than 1.5 to 2 fold during combustion, and the radiative energy flux was higher for semi-coke than coal by about 16%–27%. The radiative energy results could be described by a semi-empirical model and an artificial neural network (ANN) model. The results showed that the errors of the ANN were less than 0.01%, and demonstrated the superiority of the ANN. This study provides guidance for subsequent research on quality-splitting conversion of combustion energy.

Key words: Radiative energy flux; Fixed-bed; Oxy-coal combustion; Artificial neural network (ANN); Energy quality-splitting conversion

https://doi.org/10.1631/jzus.A1800648 **CLC number:** TK16

1 Introduction

At present, the world's energy supply is met mostly by the combustion of various fuels (Dincer and Zamfirescu, 2014). Thus, improving combustion conversion efficiency could save energy and reduce pollution. Fuel combustion generates very high temperatures and a considerable amount of radiative energy is released according to Planck's law (Böckh and Wetzel, 2012). Therefore, a concept of quality-splitting conversion of photo and thermal energy in fuel combustion was proposed (Shan et al., 2019) in which the radiation energy is separated from the thermal energy and is utilized based on different frequencies (Stanley et al., 2016; Shan and Zhou, 2019). High-frequency radiation is used for photovoltaic power generation, and low-frequency radiation and the waste heat generated during the combustion process can be recycled to achieve quality-splitting conversion of fuel combustion energy. Furthermore, this may be applied to photovoltaic/thermal power generation (Tyagi et al., 2012), photovoltaic/hot water heating (Barbieri et al., 2012), photovoltaic/refrigeration (Long et al., 2016), and photovoltaic/thermoelectric (semiconductor temperature difference) power generation (Da et al., 2016). Fig. 1 shows this concept intuitively.

Of the fuels used in quality-splitting conversion, it is important to research efficient coal combustion

‡ Corresponding author

* Project supported by the China Scholarship Council (No. 201806320236), the Zhejiang University Academic Award for Outstanding Doctoral Candidates (No. 2018071), and the Ningxia Provincial Key Research and Development Program of China (No. 2018BCE01004)

ORCID: Shi-quan SHAN, https://orcid.org/0000-0001-6635-7625

© Zhejiang University and Springer-Verlag GmbH Germany, part of Springer Nature 2019

(Liu et al., 2017) since coal is the main energy source in many developing countries such as China (Rao et al., 2015), and supports economic development of the country. In addition, pyrolysis-based coal poly-generation technology produces pyrolysis gas, coal tar, and semi-coke (Zhou et al., 2018). Semi-coke is used primarily as the fuel for combustion (Ge et al., 2017) and also requires efficient combustion conversion.

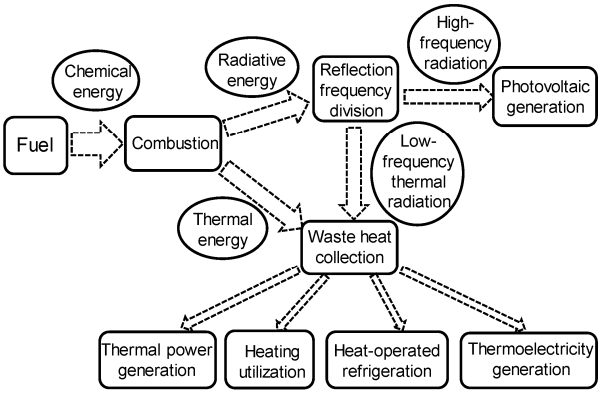

Fig. 1 Concept of energy quality-splitting conversion in fuel combustion

One of the basic coal combustion devices is the grate furnace (Rajh et al., 2018), which is a fixed-bed combustion furnace with strong adaptability for burning solid fuels such as coal, semi-coke, biomass, and waste (Sefidari et al., 2014). Therefore, research on solid fuel combustion in fixed beds has practical and general significance (Green and Waite, 2017). A tube furnace reactor in a laboratory is suitable for simulating the operation of fixed-bed devices on a small scale to investigate the combustion characteristics of solid fuels. A large number of solid fuel combustion experiments in tube furnaces have been performed to study flue gas release (Liu et al., 2018), pollutant emissions (Xu et al., 2018), and thermogravimetric characteristics (Zhang et al., 2018). However, research is lacking on the radiative energy characteristics of this combustion mode.

One way to generate higher temperatures in a combustion quality-splitting conversion system is to increase the oxygen concentration during combustion (Liu et al., 2013). Moreover, oxy-fuel combustion in an O_2/CO_2 atmosphere enriches the CO_2 in the flue gas and suppresses NO_x emission (Yin and Yan, 2016). Therefore, energy efficiency and clean utilization can be achieved through energy quality-splitting conversion during oxy-coal combustion. There have been many studies on the kinetic characteristics (Zhou et al., 2013), pollutant emissions (Vodička et al., 2018), and system efficiency (Yörük et al., 2018) of oxy-fuel combustion, but few devoted to energy quality-splitting conversion in oxy-fuel combustion.

Basic research in thermal engineering relies mostly on experiments, numerical simulations, and theoretical models. The artificial neural network (ANN) method has been increasingly applied in basic thermal engineering studies in recent years, but focused mainly on applications to state diagnosis (Zhou et al., 2017; Wang et al., 2018). Theoretically, thermal engineering problems could be modeled by an ANN using experimental data. Therefore, it is meaningful to model radiative energy characteristics through an ANN for comparison with a theoretical model.

Against this background, the objectives of this study were: (1) to investigate the radiative energy flux characteristics of oxy-coal fixed-bed combustion from the perspective of radiative energy utilization, and to provide a reference for the application of a quality-splitting conversion system based on solid fuel combustion; (2) to compare two modeling methods, a semi-empirical model and an ANN model, in combustion radiative flux research, and to provide the basis for ANN applications in subsequent research. Therefore, the one-dimensional radiative energy flux characteristics of oxy-coal combustion in a small fixed-bed furnace were first investigated under different combustion conditions. Second, the coal combustion radiative energy flux in the fixed-bed furnace was described by a semi-empirical model based on heat transfer theory. Finally, an ANN was trained to describe the experimental results, and the two methods were compared to demonstrate the feasibility of the ANN to predict the radiative energy flux. Compared to previous studies, the innovations of this study were: (1) the backgrounds were different, the concept of quality-splitting conversion of combustion energy is proposed, and current research results serve the grading conversion of photo and thermal energy in coal combustion; (2) the research objectives were different, and this study focused on the radiative energy characteristics in pulverized coal

combustion and oxy-coal combustion from the perspective of radiative energy utilization; (3) the analysis methods were diverse. This study was not only an experimental report. Two modeling methods were also investigated based on experimental data, providing a basis for the application of ANN in subsequent research.

2 Experimental and modeling methods

2.1 Experiment

Chinese Shenhua bituminous coal, which is used extensively in Chinese power plants, was crushed, ground, and sieved to obtain a coal sample with a particle size range of 75–150 μm (100–200 meshes). The sample was dried at 105 °C for 2 h. Table 1 shows the results from proximate and ultimate analyses of the coal. The bituminous pyrolysis semi-coke was prepared in a high-temperature tube furnace at a pyrolysis temperature range of 800–1200 °C with 100 °C increments. Pyrolysis continued for 30 min under an N_2 atmosphere. The oxy-fuel combustion experiment was carried out in the same tube furnace. The experimental system is shown in Fig. 2 and included a gas-mixing system, high-temperature tube furnace device, and a radiative intensity acquisition instrument. The half-length of the furnace was 30 cm, the distance between the sample center and the quartz tube outlet was 70 cm, and the tube diameter was 8 cm. The radiative sensor was 90 cm from the sample center. A CT-20 high-temperature radiative sensor (Captec Company, France) was used to monitor the total radiative intensity at a wavelength range of 0.3–50 μm, which covers most of the radiative energy spectrum. The sensor had a fast response time of 0.025 s. The experimental data were recorded using a Daq5300 eight-channel data logger (Fourier Company, Israel) with an acquisition interval of 1 s. The sensor measured the radiative intensity at a point to reflect the qualitative effects of experimental conditions on radiation. In addition, the control variable method was adopted in this study. Since many factors affect the radiation, this research focused only on the influence of the experimental factors on radiative intensity, while other factors remain unchanged under different experimental conditions. The oxy-fuel combustion experiment used O_2/N_2 and O_2/CO_2 atmospheres and five oxygen concentrations of 21%, 30%, 40%, 50%, and 60%, respectively, at a temperature of 1000 °C. The oxy-fuel condition of a 30% O_2/CO_2 atmosphere has been widely used as an alternative to air conditioning (Bejarano and Levendis, 2008). Therefore, under this atmosphere, we investigated the radiative energy flux of coal at a temperature range of 800–1200 °C with 100 °C increments, and the radiative energy flux of different semi-cokes at a temperature of 1000 °C.

At the start of the experiment, the tube furnace was heated to the required experimental temperature. The reaction atmosphere flowed through the quartz tube for 20 min at a flow rate of 1.5 L/min to ensure the appropriate experimental conditions were met. Subsequently, the empty combustion boat was quickly pushed into the center of the high-temperature reaction zone and the radiative intensity data were recorded as a calibration group representing the furnace background radiation. After the calibration experiment was completed, the same combustion boat containing the pulverized coal was quickly

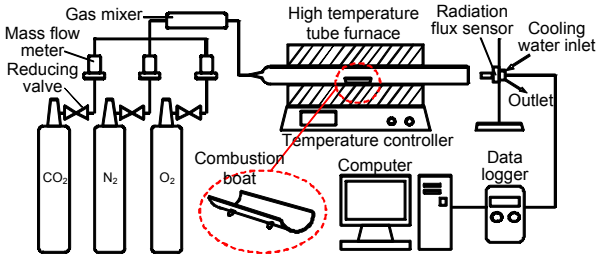

Fig. 2 Schematic diagram of the experimental system

Table 1 Proximate and ultimate analyses of the Shenhua bituminous coal

Proximate analysis				Ultimate analysis					$Q_{net,ad}$ (J/g)
M_{ad} (%)	A_{ad} (%)	V_{ad} (%)	FC_{ad} (%)	C_{ad} (%)	H_{ad} (%)	N_{ad} (%)	S_{ad} (%)	O_{ad} (%)	
6.36	5.14	30.23	58.27	70.37	3.71	1.53	0.40	12.49	27 646

Note: ad indicates air dry basis; M indicates moisture content; A indicates ash content; V indicates volatile content; FC indicates fixed carbon; Q_{net} indicates net calorific value

pushed into the reaction zone and represented the experimental group. In the experiment, 1.5 g of pulverized coal was accurately weighed and evenly spread on the bottom of the cold combustion boat. The experimental combustion boat was specially constructed and the wall surfaces at both ends were removed to monitor the radiation (Fig. 2). The difference between the experimental group results and the calibration group results was calculated to reflect the radiative energy flux caused by the coal combustion. The experiments were performed in a dark room to minimize environmental influences. In addition, to determine the uncertainty of the radiative energy results, measurements were made three times to give an average and a standard deviation represented in the figures by error bars.

2.2 Semi-empirical prediction model

Based on radiation heat transfer theory and the experimental data, we attempted to develop a semi-empirical model for predicting the radiative energy flux of coal combustion in the tube furnace. This modeling method has been used to research and analyze similar combustion processes. According to the experimental results, it appears that different combustion conditions influence emissivity. Therefore, the total radiative energy flux per unit time R can be expressed as (Modest, 2013):

$$R=\varepsilon\sigma_{\mathrm{s}}T^{4}, \tag{1}$$

where σ_{s} is the Stefan-Boltzmann constant, and T is the temperature. In solid fuel combustion, it is considered that the main effects on radiation are the triatomic gas and the solid particles resulting from incomplete combustion. Thus, the total emissivity ε can be defined as the weighted average of the gas and solid:

$$\varepsilon=k(x\varepsilon_{\mathrm{g}}+y\varepsilon_{\mathrm{s}}), \tag{2}$$

where k is a coefficient, ε_{g} and ε_{s} are the emissivities of the mixed gas and solid particles, respectively, x and y are the weights of the gas emissivity and solid emissivity, respectively, and $x+y=1$.

The weighted sum of gray gases (WSGG) model is a classical gas emissivity model, one of many developed models of oxy-fuel conditions (Kangwanpongpan et al., 2012; Shan et al., 2017). The WSGG model was used to calculate ε_{g}. The core concept of the WSGG model is to replace the actual non-gray gas with n gray gases. The weighted sum of the absorption coefficient or radiative heat flux of each gray gas is equal to the total value of the actual gas. The gas emissivity over the path-length L is expressed as:

$$\varepsilon=\sum_{i=1}^{n}a_i\left[1-\exp(-\kappa_i XpL)\right], \tag{3}$$

where X is the ratio of the triatomic gas, expressed as the sum of the mole fractions of H_2O and CO_2. p is the pressure. The absorption coefficient κ_i of each gray gas is constant in a certain spectral region and the weight a_i indicates the ratio of black body radiation in this spectral region. The sum of the weights must be 1, which also includes the weight a_0 of the white gas, and the corresponding absorption coefficient κ_0 is 0. Here, a_i is related mainly to the temperature and the molar ratio R_{m} of H_2O/CO_2, and κ_i is dependent mainly on R_{m}. Therefore, if the parameters such as the molar fraction of the triatomic gases X, the molar ratio R_{m}, the average temperature T, and the path-length L are obtained, the mixed gas emissivity can be calculated using the WSGG model.

In this study, the WSGG model of Shan et al. (2018) was selected, which was developed for oxy-fuel conditions and covers a wide range of gas media conditions. The path-length L was 70 cm from the furnace center to the tube outlet in the experiment, and the average temperature was used. Fig. 3 shows the temperature distribution in the tube furnace measured using a K-type thermocouple. The temperature at the outlet was assumed to be ambient. Thus, it could be assumed that the temperature decreased linearly in multiple stages from the furnace center to the tube outlet. Consequently, the temperature at each stage was weighted and averaged to calculate the average temperature in the entire path-length. After the preliminary calculation, the weighted average temperatures under the different temperature conditions in the range of 800–1200 °C were 357.14, 407.14, 457.14, 528.57, and 600 °C, respectively. These values were used for the WSGG model calculation. The molar fraction of the triatomic gas X and the molar ratio R_{m} were calculated for the different atmospheric conditions and the coal ultimate analysis

under the assumption of complete combustion. Subsequently, the gas emissivity ε_g was obtained.

There was a large amount of dark smoke in the initial stage. Because the radiation of the soot particles involves complex scattering (Modest, 2013), the extinction coefficient of the particles was large and the smoke shielded most of the radiation in the current experimental condition. Thus, the emissivity of the soot should be small and its variation under different conditions not large. Therefore, the emissivity of the soot particles ε_s was assumed to be 0.1 in the preliminary semi-empirical model, which is smaller than the gas emissivity. In addition, the weight of particle emissivity y was used to reflect the variation in particle radiation under different conditions. To obtain more accurate soot characteristics, laser measurements should be used in future research.

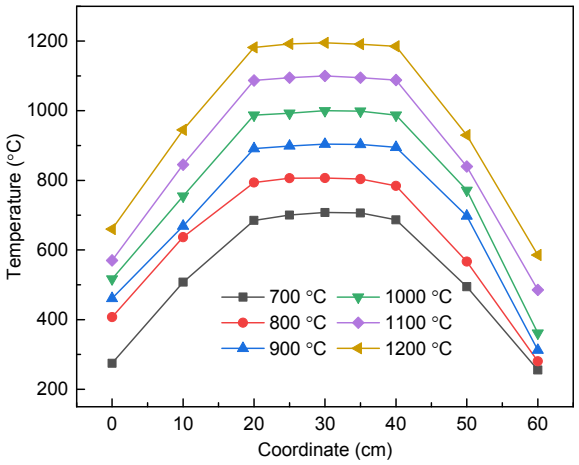

Fig. 3 Tube furnace temperature calibration curves (the coordinate at 30 cm is the furnace center)

2.3 ANN model

An ANN is an information-processing technique that is widely used in scientific research and engineering practice. The radial basis function (RBF) network has advantages in function approximation and system model construction (Esfe, 2017). Thus, it was used in this study to train the experimental data, and a prediction model was established to describe the combustion radiative flux characteristics.

The RBF network is a feed-forward network composed of three layers. The method has been shown to have uniform approximation performance for nonlinear networks. The generalized RBF network structure is shown in Fig. 4.

The generalized RBF network has M input nodes, namely M training samples. The hidden layer has I nodes and $I<M$. The basis function of the ith hidden node is $\Phi(\|\boldsymbol{X}_m, \boldsymbol{X}_i\|)$, where $\|\boldsymbol{X}_m, \boldsymbol{X}_i\|$ refers to the Euclidean norm, $\boldsymbol{X}_m=[x_1, x_2, \ldots, x_M]$ is input sample, and $\boldsymbol{X}_i=[x_{i,1}, x_{i,2}, \ldots, x_{i,M}]$ is the center of the basis function. The threshold Φ_0 is added to the hidden layer. Its output is always 1 and the weight connected to the output unit is $\omega_{0,j}$. The output layer has J neurons.

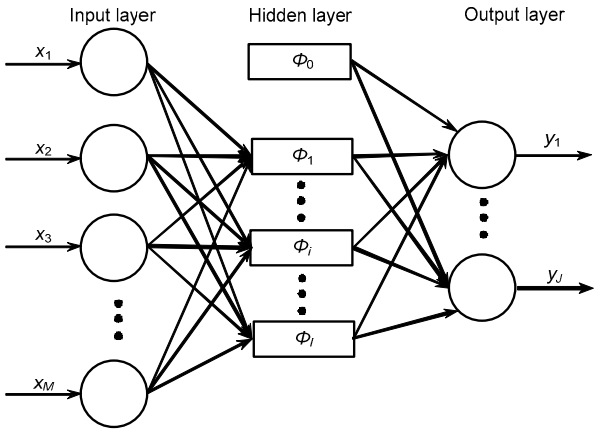

Fig. 4 RBF network structure diagram

We set the actual output as $\boldsymbol{Y}=[y_1, y_2, \ldots, y_J]$, where J is the number of output units. For the training sample $\boldsymbol{X}_m$, the jth output unit result is

$$y_j = \omega_{0,j} + \sum_{i=1}^{I} \omega_{i,j} \Phi(\boldsymbol{X}_m, \boldsymbol{X}_i). \tag{4}$$

The basis function is generally a Gaussian function, thus:

$$\begin{aligned} \Phi(\boldsymbol{X}_m, \boldsymbol{X}_i) &= \Phi(\|\boldsymbol{X}_m - \boldsymbol{X}_i\|) \\ &= \exp\left(-\frac{1}{2\sigma^2}\|\boldsymbol{X}_m - \boldsymbol{X}_i\|\right). \end{aligned} \tag{5}$$

The RBF algorithm is a mature algorithm. In this study, an RBF network was designed using the 'newrb' function in Matlab software to train the experimental data. A model describing the relationship between the total radiant energy flux and the different combustion conditions was established and tested using typical experimental data.

3 Results and discussion

3.1 Effect of different conditions on the radiative energy

3.1.1 Different atmospheres

Fig. 5 shows the variation in the radiative intensity detected during a period of 360 s after the combustion boat entered the tube. The results show that the radiative intensity curve after 300 s closely matched the calibration curve of the empty combustion boat, which indicates that the reaction was almost complete. Thus, we investigated the radiative energy flux during the period of 360 s. The radiative intensity decreased during the initial 20 s due to the operational disturbance after the combustion boat was placed in the furnace. Subsequently, the reaction process was divided into three stages (Fig. 5). During the first stage, the combustion reaction begins and the soot volatiles are released from 21 s to 45 s (stage 1). The second stage is the soot diffusion and burnout stage, from about 45 s to 90 s (stage 2). The third stage is the coal char burnout stage, after about 90 s (stage 3).

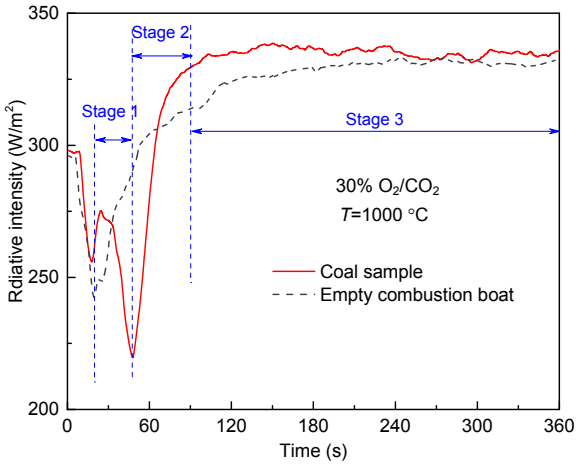

Fig. 5 Comparison of the radiative energy flux curves of the calibration (empty combustion boat) and experimental data (coal sample)

The experiment used a high-volatility bituminous coal. A large amount of smoke was generated after the combustion boat was placed in the reactor. The soot particles had an extremely large extinction coefficient due to the scattering effect. Thus, they shielded the flame radiation and the emissivity was low. In addition, the average media temperature was not high in the tube, so the radiative intensity of the soot media was low. Therefore, the radiative intensity was considered to be zero when the radiation curve was lower than the calibration curve.

Fig. 6a shows the total calculated radiative energy flux from 21 s to 360 s in the O_2/CO_2 and O_2/N_2 atmospheres. The radiative energy flux increased in both combustion atmospheres as the oxygen concentration increased. This was attributed mainly to a reduction in the emission of soot and volatiles, as well as the increase in the coal combustion temperature. Therefore, increasing the oxygen concentration helped to enhance the proportion of radiative energy in the combustion energy grading conversion system.

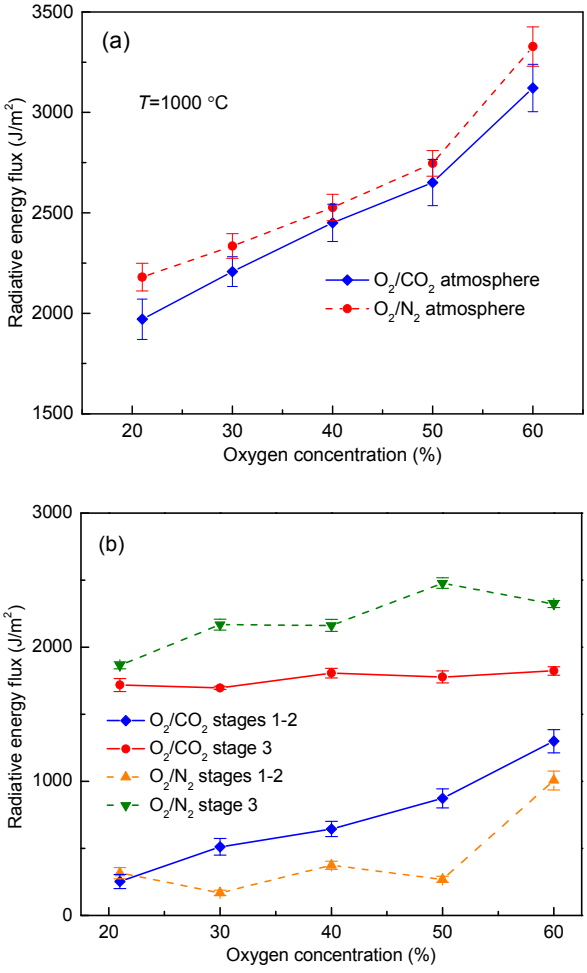

Fig. 6 Radiative energy flux for different oxygen concentrations in two atmospheres
(a) Total process; (b) Stages 1–2 and stage 3

Fig. 6b shows the radiative energy flux at the soot volatile release and burnout stages (stages 1–2) and the char burnout stage (stage 3). The radiative energy flux increased greatly with the oxygen concentration in stages 1–2, whereas it changed little in the char burnout stage (stage 3). This indicates that the oxygen concentration affects mainly the volatile release and burnout process, and influences the changes in the total radiative energy flux. In practice, the method of increasing the oxygen concentration is more helpful to increase the proportion of radiative energy of high volatile fuels. Furthermore, the radiative energy flux was higher in the O_2/CO_2 atmosphere than in the O_2/N_2 atmosphere in stages 1–2. This indicates that volatiles and soot were released and burned faster, and that this process required less time in the O_2/CO_2 atmosphere. Thus, the radiative energy flux was shielded for a shorter period. As the oxygen concentration increased to 60%, there was less difference in the radiative energy flux between the two atmospheres in stages 1–2. In the char burnout stage (stage 3), the radiative energy flux was higher in the O_2/N_2 atmosphere than in the O_2/CO_2 atmosphere. This occurred primarily because of differences in the specific heat capacity and radiative characteristics of the two atmospheres, causing the combustion temperature to be slightly higher in the O_2/N_2 atmosphere (Andersson et al., 2008). For the entire process, the radiative energy did not differ significantly between the two atmospheres, although it was slightly higher under O_2/N_2 conditions.

The change rate is defined as the variation of the radiation intensity per unit time, and its unit is W/(m^2·s). The average change rate of radiative intensity v is its average value in a certain period. Fig. 7 shows the average change rate v_1 in stage 1 (volatile and soot release) and v_2 in stage 2 (volatile and soot burnout). Here, v_1 is negative and represents the reduction rate in stage 1, while v_2 is positive and represents the growth rate in stage 2. In the O_2/CO_2 atmosphere, the radiation reduction rate v_1 gradually changed from −3.5 W/(m^2·s) to −1.65 W/(m^2·s) as the oxygen concentration increased from 21% to 60%, whereas the radiation growth rate v_2 was reduced from 2.7 W/(m^2·s) to 0.5 W/(m^2·s). The results were similar for the O_2/N_2 atmosphere in that the absolute value of v_1 was reduced by about 2 W/(m^2·s), whereas v_2 was reduced by about 1.5 W/(m^2·s). This occurred primarily because the soot combustion consumption rate was enhanced and the soot particles reduced as the oxygen concentration increased in stages 1–2. Therefore, there was less shielded radiative energy and the average change rate was small.

Fig. 7 also demonstrates that the average change rates of stage 1 and stage 2 were higher in the O_2/CO_2 atmosphere than in the O_2/N_2 atmosphere. This was caused primarily by the slow diffusion rate of the O_2 in the CO_2 atmosphere. More volatiles were released, but they did not burn out rapidly. Thus, there was much more soot and the radiative intensity decreased rapidly. In addition, after the volatiles were released in the O_2/CO_2 atmosphere, the active sites on the coal char were exposed to promote the CO_2 gasification reaction (Gao et al., 2013), which also accelerated the entire pyrolysis and combustion processes.

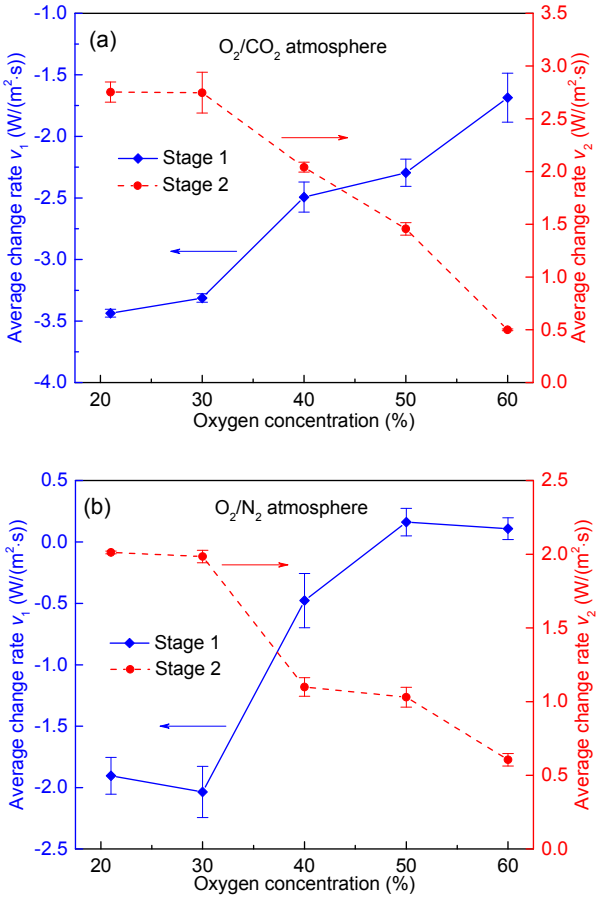

Fig. 7 Average change rates of the radiative intensity in stage 1 and stage 2
(a) O_2/CO_2 atmosphere; (b) O_2/N_2 atmosphere

3.1.2 Different temperatures

Fig. 8a shows the radiative energy flux of the bituminous coal combustion under 30% O_2/CO_2 oxygen-fuel conditions. The radiative energy flux increased about two fold from about 1400 J/m^2 to 3900 J/m^2 as the temperature increased from 800 °C to 1200 °C. According to Planck's law, the temperature directly affects the surface radiative intensity of a black body. Thus, solid and gas radiation media have greater radiation intensity in a high-temperature combustion. Therefore, elevating the system temperature is the key to improving the performance of quality-splitting conversion of the combustion energy in practical applications. Specifically, a flue gas heat regenerator, an insulated furnace, high calorific value fuel, and oxy-enriched combustion could be used. Fig. 8a shows the radiative energy flux during the volatile release and burnout processes (stages 1–2) and the coal char burnout process (stage 3), both of which increased with the combustion temperature. In addition, the radiative energy released in stage 3 accounted for about 78.6%–84.6% of the total energy. Therefore, the total radiative energy flux variation is determined by the char burnout process.

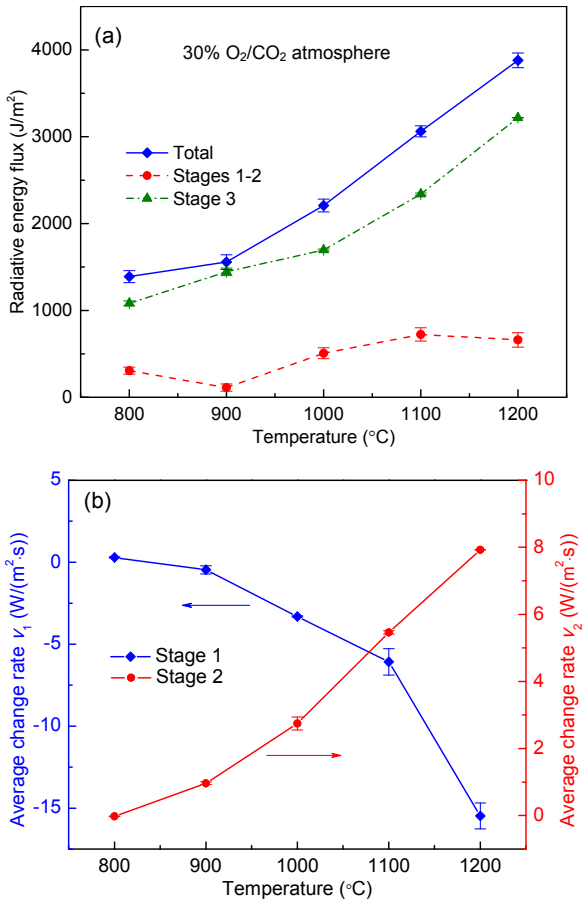

Fig. 8 Effect of temperature on the radiative energy flux (a) and the average radiative intensity change rate (b) in an oxy-coal combustion

Fig. 8b shows the average change rate of the radiative intensity v_1 for stage 1, and v_2 for stage 2, at different temperatures. As the temperature increased from 800 °C to 1200 °C, the reduction rate v_1 changed from 0 to −15 W/(m^2·s), whereas the growth rate v_2 increased from 0 to 8 W/(m^2·s). This indicates that the radiative intensity change rate at each reaction stage increased with temperature. This occurred because the temperature increase promoted the volatile pyrolysis and soot release process under the 30% O_2/CO_2 atmosphere. Moreover, a larger amount of volatiles and soot were released, and released more rapidly, at the higher temperatures in the initial combustion.

3.1.3 Different fuels

Fig. 9a shows the radiative energy flux and radiation efficiency of 30% O_2/CO_2 oxy-fuel combustion for the semi-cokes at different pyrolysis temperatures. The combustion temperature was 1000 °C. The radiation efficiency η is the ratio of the radiative energy in the combustion to the calorific value of the fuel (Turns, 2012):

$$\eta = R/Q, \tag{6}$$

where the radiative energy R is calculated from the amount of radiative energy flux on the cross-sectional area of the tube furnace, and Q is the energy contained in the fuel. Note that R is not the entire radiative energy in the coal combustion in this study, so the radiative efficiency η may be lower. However, a comparison of the radiation efficiency shows that there is an effect of the combustion conditions on the proportion of radiative energy. The results of the measured calorific values of the semi-cokes at five different pyrolysis temperatures are shown in Table 2.

Not a large amount of heavy smoke was released in the combustion since the semi-coke had undergone a pyrolysis process. Therefore, there was no significant decrease in radiative intensity at the beginning of the combustion. Fig. 9a shows that the radiative

energy flux was higher for the semi-coke than for the coal by about 16%–27%. This also confirms that the release of the volatiles and soot shielded the radiative energy flux in the coal combustion, and that low-volatile fuels made more sense for systems involving quality-splitting conversion of combustion energy. Fig. 9 also shows that the high-temperature pyrolysis of the semi-coke resulted in a significantly higher radiative energy flux. The radiative energy flux of the semi-coke from the 1200 °C pyrolysis was about 300 J/m^2 higher than that of the semi-coke from the 800 °C pyrolysis. More volatiles were released in the higher-temperature pyrolysis; therefore, the semi-coke contained more char for the same mass. There were more luminescent carbon and soot particles, and CO_2 gas was generated in the semi-coke combustion, which increased the proportion of radiative energy flux. In contrast, the semi-coke with a relatively low pyrolysis temperature still contained a portion of the volatiles released during the pyrolysis stage. The radiative intensity decreased if the volatiles were not completely burned.

Table 2 Calorific values of semi-coke at different pyrolysis temperatures

Pyrolysis temperature (°C)	Calorific value (J/g)
800	29288.3
900	28870.9
1000	28863.8
1100	27930.7
1200	28029.7

Fig. 9a shows that the radiation efficiency of semi-coke combustion increased with the pyrolysis temperature, and was also higher than that of raw coal. This was consistent with the trend in the radiative energy flux. The semi-coke had a radiation efficiency of 0.029% at a pyrolysis temperature of 800 °C, and about 0.034% at a pyrolysis temperature of 1200 °C. This indicates that higher pyrolysis temperature resulted in a larger proportion of radiative energy in the combustion. In addition, semi-cokes have different surface radiation characteristics because they have different surface structures at different pyrolysis temperatures (Zhou et al., 2014). A semi-coke at a higher pyrolysis temperature should have greater emissivity due to a more porous structure. Pyrolysis above 800 °C is considered high-temperature pyrolysis, which is used mainly for the poly-generation of pyrolysis gas and semi-coke. The results show that the semi-coke had a larger proportion of radiative energy at high-temperature pyrolysis. Therefore, poly-generation semi-coke is more suitable for the quality-splitting conversion of combustion energy and this approach can be combined with the pyrolysis poly-generation process to create an efficient coal grading conversion scheme.

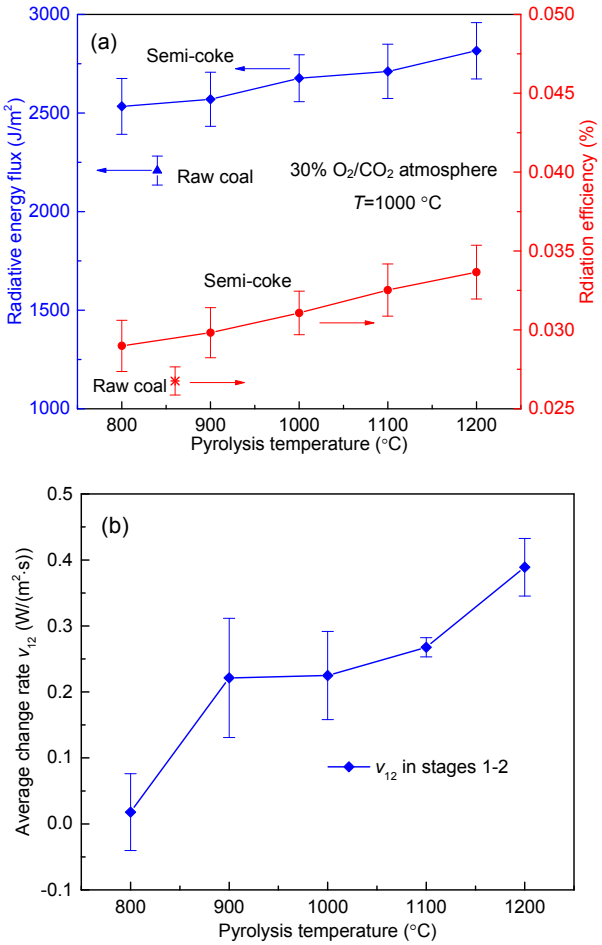

Fig. 9 Effect of pyrolysis temperatures on radiative energy flux and radiation efficiency (a), and average radiative intensity change rate (b) in 30% O_2/CO_2 combustion of semi-coke

Fig. 9b shows the average change rate v_{12} of the radiative intensity under different semi-coke conditions, where v_{12} is defined as the average change rate of radiative intensity both in the volatile release stage (stage 1) and in the burnout stage (stage 2). Compared

to coal combustion, the average change rate was low and less than 0.4 W/(m^2·s) for the semi-coke, because the volatiles had mostly been released. As v_{12} was positive, the radiative intensity increased in stages 1–2. Moreover, v_{12} showed an overall upward trend as the pyrolysis temperature increased. This may have been because at a lower pyrolysis temperature, the semi-coke released some volatiles in the initial combustion stage, which affected the increase in radiative intensity. On the other hand, semi-cokes at different pyrolysis temperatures have different pore structures, which should also affect the rate of increase in combustion radiative energy.

3.2 Semi-empirical prediction model results

As described in Section 2.2, a semi-empirical radiative energy prediction model was developed. Using the entire reaction process as a unit of time, the radiative energy flux of the oxy-coal combustion in a tube furnace can be predicted using Eqs. (1) and (2). The relevant parameters were determined based on the experimental results. First, the gas emissivity ε_g for each condition was calculated using the WSGG model. As described above, the soot emissivity ε_s was 0.1 in the model, which was lower than the gas emissivity. In Eq. (2), k was set to 1.1 so that different conditions were suitable. The soot emissivity weight y was determined by Eqs. (1) and (2) according to ε_s and the measured radiative energy flux. Therefore, the modeling focus was to determine the relationship between y and the experimental conditions. The experimental results indicate that there were fewer volatiles and less soot released during combustion at higher oxygen concentration or lower temperature. Therefore, y is considered to be proportional to the temperature and inversely proportional to the oxygen concentration φ. A linear equation with two unknowns is introduced here to approximate this relationship:

$$y = A + B\varphi + CT + DT\varphi, \tag{7}$$

where A, B, C, and D are fitting coefficients.

Using the radiative energy flux data under different oxygen concentrations in an O_2/CO_2 atmosphere and the data for different temperatures in a 30% O_2/CO_2 atmosphere, nonlinear curve fitting was performed using Origin software and the Levenberg-Marquardt optimization algorithm. The results are listed in Table 3.

Table 3 Fitted parameters of the soot emissivity ratio y in the prediction model

Atmosphere	A	B	C	D
O_2/CO_2	11 227.73	−374.24	−8.817 93	0.293 94
O_2/N_2	1.123 390	−0.015 491	0	0

The radiative energy flux was calculated based on the O_2/CO_2 atmosphere parameters in Table 3 and Eqs. (1) and (2), and the calculated results were compared with the experimental data shown in Figs. 10a and 10b. The established model results were consistent with the experimental data trend. Fig. 10a shows that the maximal model error was about 7%. Fig. 10b shows that the model error was about 12% at 900 °C and less than 5% at other temperatures. Since the semi-empirical model is a mathematical function and its results show a smooth curve, there are always errors between the experimental results and the model results. Although the model errors were different under various conditions, the semi-empirical model could still describe the trend of the results.

For the O_2/N_2 atmosphere condition of different oxygen concentrations at a combustion temperature of 1000 °C, the ratio y was still inversely proportional to the oxygen concentration. According to Eq. (7), it was observed that y had a linear relationship with the oxygen concentration φ at a constant temperature, i.e. $y=A+B\varphi$. After calculating the y values of different oxygen concentrations in the O_2/N_2 atmosphere, a linear fit was performed (Fig. 11a). The parameters are listed in Table 3. The calculated results and the experimental results are shown in Fig. 10c. The calculated results agreed well with the experimental data, and the model error did not exceed 5%.

A sensitivity and significance analysis of the regression model was performed. Soot emissivity ε_s and the coefficient k were enhanced and reduced by 10%, respectively, while other parameters were unchanged. The adjusted model was then used to predict the results of Fig. 10a. The current model was used as a control group, and the model fitting deviation was analyzed as shown in Table 4 (p.442). The fitting deviation was related to the absolute ε_s variation value, and did not exceed 10%. It was consistent

with the variation of k. This is because the semi-empirical model relies on theory and experimental results. Thus, if ε_s or k changes, the regression formula Eq. (7) should be re-regressed based on the experimental results to ensure accurate description of the experimental data.

To evaluate the ability of regression models to describe objective experimental results, the model significance was analyzed (Table 5). For the O_2/CO_2 atmosphere, the model constructed by Eq. (7) was used to describe the experimental results in Figs. 10a and 10b. As F=125.57>$F_{0.01}$(2, 6), the regression model was significant at the level of α=0.01. Its standard deviation σ was 148.84. Thus, there was a 99% probability that the error did not exceed 2σ=297.68 J/m^2. For the O_2/N_2 atmosphere, the regression model was used to describe the experimental results in Fig. 10c. As F=30.92>$F_{0.05}$(1, 3), the regression model was significant at the level of α=0.05, and its standard deviation σ was 153.12 J/m^2.

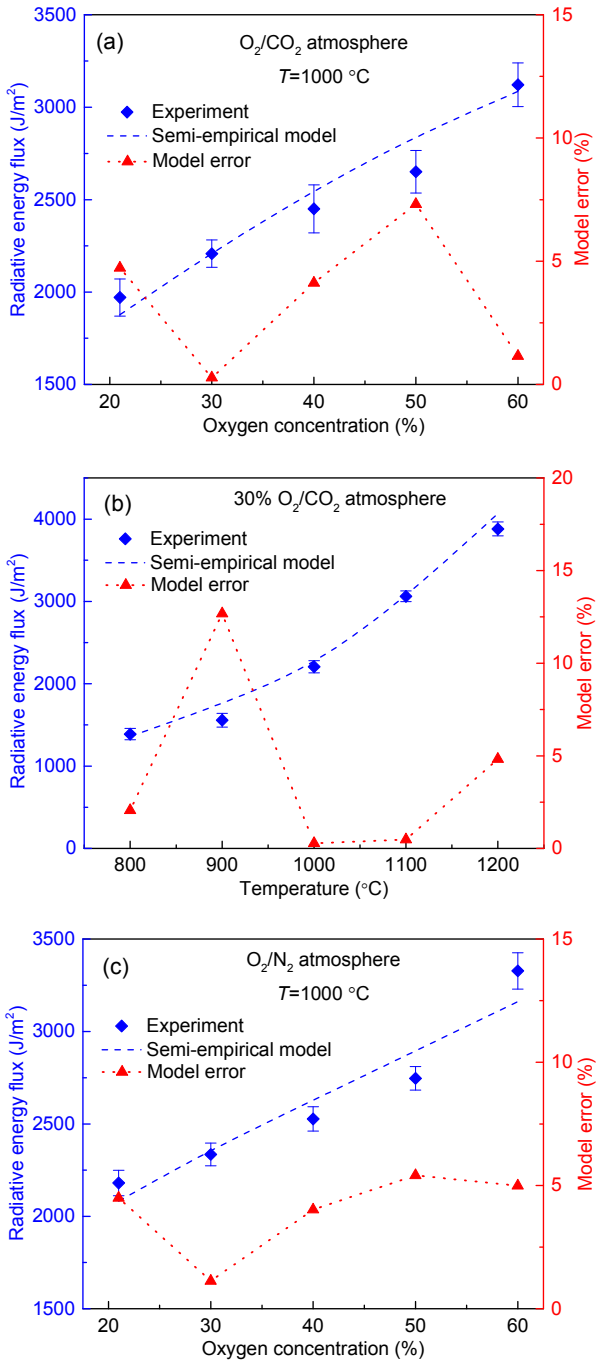

Fig. 10 Comparison of experimental results and model-calculated results of the radiative energy flux
(a) Different oxygen concentrations (O_2/CO_2 atmosphere); (b) Different combustion temperatures; (c) Different oxygen concentrations (O_2/N_2 atmosphere)

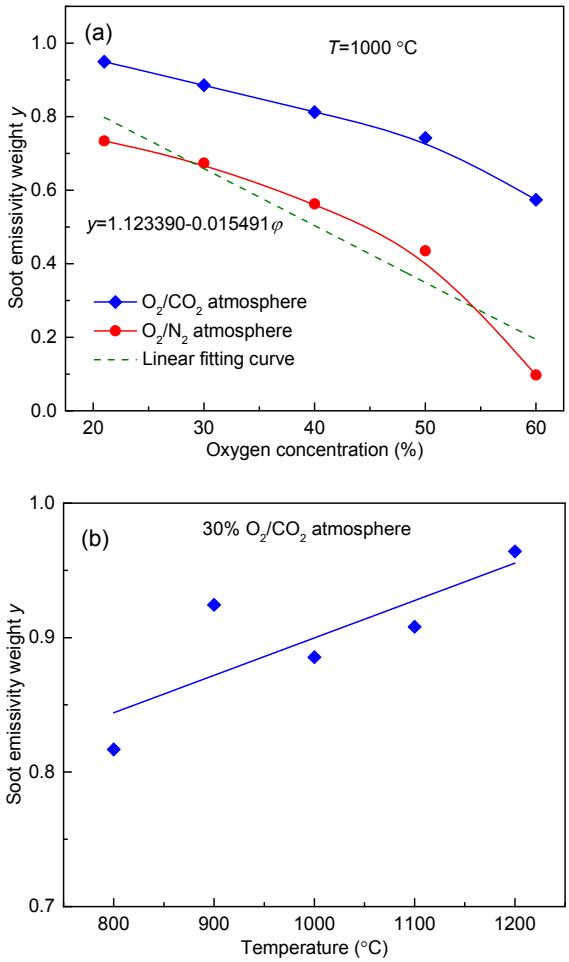

Fig. 11 Soot emissivity weight y in the model at different oxygen concentrations (O_2/CO_2 and O_2/N_2 atmospheres) (a) and different combustion temperatures (30% O_2/CO_2 atmosphere) (b)

Table 4 Sensitivity analysis of the model fitting deviation

Condition	Model fitting deviation (%)					
	Soot emissivity ε_s			Coefficient k		
	Level 1 (+10%)	Control group	Level 2 (−10%)	Level 1 (+10%)	Control group	Level 2 (−10%)
21% O_2/CO_2	9.197	0	9.197	10	0	10
30% O_2/CO_2	7.082	0	7.082	10	0	10
40% O_2/CO_2	5.454	0	5.454	10	0	10
50% O_2/CO_2	4.271	0	4.271	10	0	10
60% O_2/CO_2	3.366	0	3.366	10	0	10

Table 5 Variance analysis of the regression model

Source		Quadratic sum	Degree of freedom	Variance	F	Significance
Computational formula	Regression	$U=\sum_{t=1}^{N}(\hat{y}_t-\overline{y}_t)^2$	K	U/K	$\frac{U/K}{\sigma^2}$	–
	Residual	$S=\sum_{t=1}^{N}(y_t-\hat{y}_t)^2$	$N-K-1$	$\sigma^2=S/(N-K-1)$		
O_2/CO_2 atmosphere: $R=f(T, \varphi)$	Regression	5 563 195.91	2	2 781 597.95	125.57	α=0.01
	Residual	132 915.92	6	22 152.65		
O_2/N_2 atmosphere: $R=f(\varphi)$	Regression	724 896.03	1	724 896.03	30.92	α=0.05
	Residual	70 339.034	3	23 446.34		

Note: K is the number of independent variables; N is the number of experimental values; U is the regression quadratic sum; S is the residual quadratic sum; y_t is the experimental value; $\overline{y}_t$ is the average experimental value; $\hat{y}_t$ is the model predicted value

Thus, there was a 95% probability that the error did not exceed 2σ=306.24 J/m^2 when the regression model was used to describe the experimental results. This indicates that the semi-empirical model established in this study for a specific combustion mode (coal fixed-bed combustion) provided good modeling results. Therefore, a similar modeling method could be used for different combustion modes to investigate the radiative energy characteristics. This is important for further studies of quality-splitting conversion of combustion energy.

Fig. 11 shows the variation of the soot emissivity weight y under different conditions. Fig. 11a shows that between the oxygen concentrations of 21% and 60%, the y value decreased by about 0.4 in the O_2/CO_2 atmosphere and by about 0.6 in the O_2/N_2 atmosphere. This indicates that there were fewer volatiles and less soot released at higher O_2 concentrations. Moreover, the y value was lower in the O_2/N_2 atmosphere, indicating that there was less soot released and the radiative energy was higher, which is consistent with the results shown in Fig. 6. Fig. 11b shows that the value of y increased by about 0.15 as the temperature increased from 800 °C to 1200 °C, which also indicates that high temperature promotes the reaction and accelerates the release of soot and volatiles.

3.3 ANN model analysis results

3.3.1 Oxygen conditions prediction model

The RBF network was used to establish a model describing the relationship between the radiative energy experimental results and the combustion conditions. For the oxygen concentrations ranging from 21% to 60% in the O_2/CO_2 conditions, the parameters were used to train the RBF network. The parameters included the total radiative energy flux R_{whole} (J/m^2), the radiative energy R_1 (J/m^2) in the soot release stage (stage 1), and the average absolute change rate of the radiative intensity v_{12} (W/(m^2·s)) in the soot release and burnout stages (stages 1–2). The training experiment data are shown in Table 6. The experimental data from different oxygen concentrations were expanded to 100 groups using cubic spline

interpolation to train the RBF network. This is a valid method for expanding training data. In the RBF network, the number of neurons was 50 and the spread coefficient was 25.

For the first mode (mode 1), five sets of experimental data were expanded for training, and five sets of experimental conditions were re-evaluated using the trained network. This mode was used to evaluate the modeling ability of the ANN and the results are shown in Fig. 12a. The five sets of oxygen concentrations predicted by the RBF network were in good agreement with the actual values, and the residuals did not exceed 0.5%. That is, the model error was less than 2.5%. This indicates that the ANN model was effective for predicting the coal combustion conditions using the radiative energy results.

For the second mode (mode 2), four datasets of 21%, 40%, 50%, and 60% oxygen concentrations, respectively, were expanded through cubic interpolation and trained using the same method. This net was then used to test the experimental data of the 30% oxygen concentration. This model was used to show the ability of the ANN to predict unknown experimental results. The predicted results are shown in Fig. 12c. The predicted oxygen concentration was 31.67% and the residual was only 1.67%. This indicates that the RBF network was suitable for predicting unknown combustion conditions.

Table 6 RBF network training data

No.	R_{whole} (J/m^2)	R_1 (J/m^2)	v_{12} (W/(m^2·s))	φ (%)
1	1970.8	253.3	2.73	21
2	2207.8	511.7	2.55	30
3	2450.3	643.9	2.14	40
4	2651.0	872.8	2.06	50
5	3121.5	1298.9	1.77	60

3.3.2 Radiative energy prediction model

For the O_2/CO_2 atmospheres at 1000 °C, the oxygen concentration conditions between 21% and 60% were used as the input and the total radiative energy flux R_{whole} was used as the output to train the RBF network (Table 6). The trained network was used to predict the total radiative energy flux.

For the first mode (mode 1), the RBF network was trained using five sets of experimental data, and the data were expanded to 100 groups using cubic spline interpolation. The number of neurons was 50 and the spread coefficient was 25. The five groups of radiative energy flux results were re-evaluated using the trained network, and the results are shown in

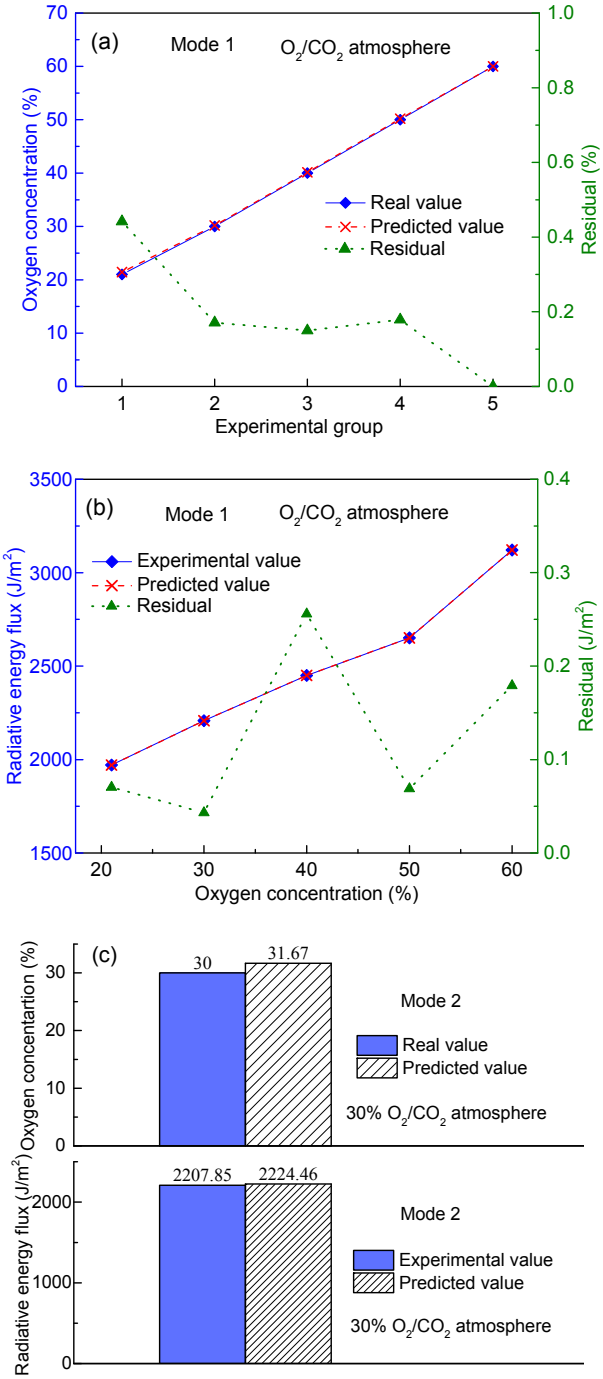

Fig. 12 RBF network prediction results: (a) mode 1 of oxygen concentration; (b) mode 1 of radiative energy flux; (c) mode 2

Fig. 12b. A comparison with the semi-empirical model results in Fig. 10a indicates that the results predicted by the RBF network were in good agreement with the experimental data, and the residuals did not exceed 0.25 J/m^2. That is, the model error was less than 0.01%. Moreover, Fig. 10a shows the maximum semi-empirical model error was about 7.5%. Therefore, the radiative energy in oxy-coal combustion can be better modeled using the ANN model than using the semi-empirical model.

For the second mode (mode 2), four datasets of 21%, 40%, 50%, and 60% oxygen concentrations, respectively, were expanded through cubic interpolation and trained using the same method. This net was used to test the radiative energy flux data of the 30% oxygen concentration. The prediction results are shown in Fig. 12c. The residual was only 16.61 J/m^2 between the predicted value of 2224.46 J/m^2 and the experimental value of 2207.85 J/m^2. This result shows that the RBF network can also be used to predict untested experimental results.

Overall, the results show that the ANN can be used to model the radiative energy flux in the combustion process and to predict untested radiative energy flux. A comparison with the semi-empirical model results indicates that the ANN is not only highly accurate, but also not limited by physical processes, so it has excellent adaptability. In addition, the ANN has a good ability to predict unknown experimental results. Therefore, this method provides a reliable means for researching the quality-splitting conversion of combustion energy.

4 Conclusions

In this study, a small-scale fixed-bed tube furnace was used to determine the one-dimensional radiative energy flux in oxy-fuel combustion for solid fuels such as coal and semi-coke, for evaluating radiative energy utilization in solid fuel combustion. Subsequently, a semi-empirical prediction model for the radiative energy flux was established based on heat transfer theory. Finally, an ANN was used to model the radiative energy flux and was compared with the semi-empirical model. The following conclusions can be drawn:

1. The volatile matter and soot released during the initial stage of solid fuel combustion was the main cause of a reduction of the radiative energy flux. Therefore, the use of low volatile fuels and oxy-enrich combustion could enhance the proportion of flame radiative energy.

2. Elevating the temperature in oxy-fuel combustion was the most important factor to enhance the proportion of radiative energy. In practice, the use of a flue gas heat regenerator, an insulated furnace, and high calorific value fuel could increase the proportion of flame radiative energy.

3. The radiative energy flux in the combustion of poly-generation semi-coke was higher than that of coal by about 16%–27%, and the semi-coke from higher-temperature pyrolysis had greater radiation energy. Therefore, an efficient coal grading conversion scheme could be created by combining coal pyrolysis poly-generation with quality-splitting conversion of semi-coke combustion energy.

4. The radiative energy in a specific combustion mode could be described both by a semi-empirical model and an ANN. The ANN had not only high accuracy, but also excellent adaptability compared with the semi-empirical model. The ANN also had a good ability to predict experimental results. Therefore, an ANN provides a reliable research method for quality-splitting conversion of combustion energy.

References

Andersson K, Johansson R, Johnsson F, et al., 2008. Radiation intensity of propane-fired oxy-fuel flames: implications for soot formation. *Energy & Fuels*, 22(3):1535-1541. https://doi.org/10.1021/ef7004942

Barbieri ES, Spina PR, Venturini M, 2012. Analysis of innovative micro-CHP systems to meet household energy demands. *Applied Energy*, 97:723-733. https://doi.org/10.1016/j.apenergy.2011.11.081

Bejarano PA, Levendis YA, 2008. Single-coal-particle combustion in O_2/N_2 and O_2/CO_2 environments. *Combustion and Flame*, 153(1-2):270-287. https://doi.org/10.1016/j.combustflame.2007.10.022

Böckh P, Wetzel T, 2012. Heat Transfer: Basics and Practice. Springer-Verlag, Berlin Heidelberg, Germany.

Da Y, Xuan YM, Li Q, 2016. From light trapping to solar energy utilization: a novel photovoltaic–thermoelectric hybrid system to fully utilize solar spectrum. *Energy*, 95:200-210. https://doi.org/10.1016/j.energy.2015.12.024

Dincer I, Zamfirescu C, 2014. Advanced Power Generation

Systems. Elsevier, Amsterdam, the Netherlands. https://doi.org/10.1016/C2009-0-63866-6

Esfe MH, 2017. Designing an artificial neural network using radial basis function (RBF-ANN) to model thermal conductivity of ethylene glycol–water-based TiO_2 nanofluids. *Journal of Thermal Analysis and Calorimetry*, 127(3):2125-2131. https://doi.org/10.1007/s10973-016-5725-y

Gao SP, Zhao JT, Wang ZQ, et al., 2013. Effect of CO_2 on pyrolysis behaviors of lignite. *Journal of Fuel Chemistry and Technology*, 41(3):257-264. https://doi.org/10.1016/S1872-5813(13)60017-1

Ge LC, Zhang YW, Wang ZH, et al., 2017. A novel power generation system based on the cascade utilization of coal: concept and preliminary experimental results. *Energy Sources, Part A: Recovery, Utilization, and Environmental Effects*, 39(19):1955-1962. https://doi.org/10.1080/15567036.2013.828133

Green AS, Waite ML, 2017. Designing chain grate stoker links to reduce polluting and particulate emissions. *Journal of the Energy Institute*, 90(3):424-430. https://doi.org/10.1016/j.joei.2016.03.007

Kangwanpongpan T, França FHR, da Silva RC, et al., 2012. New correlations for the weighted-sum-of-gray-gases model in oxy-fuel conditions based on HITEMP 2010 database. *International Journal of Heat and Mass Transfer*, 55(25-26):7419-7433. https://doi.org/10.1016/j.ijheatmasstransfer.2012.07.032

Liu LL, Kumar S, Wang ZH, et al., 2017. Catalytic effect of metal chlorides on coal pyrolysis and gasification part I. Combined TG-FTIR study for coal pyrolysis. *Thermochimica Acta*, 655:331-336. https://doi.org/10.1016/j.tca.2017.07.007

Liu LL, Yuan Y, Kumar S, et al., 2018. Catalytic effect of metal chlorides on coal pyrolysis and gasification part II. Effects of acid washing on coal characteristics. *Thermochimica Acta*, 666:41-50. https://doi.org/10.1016/j.tca.2018.06.001

Liu X, Chen MQ, Yu D, 2013. Oxygen enriched co-combustion characteristics of herbaceous biomass and bituminous coal. *Thermochimica Acta*, 569:17-24. https://doi.org/10.1016/j.tca.2013.06.037

Long R, Li BD, Liu ZC, et al., 2016. Performance analysis of a solar-powered electrochemical refrigerator. *Chemical Engineering Journal*, 284:325-332. https://doi.org/10.1016/j.cej.2015.09.021

Modest MF, 2013. Radiative Heat Transfer, 3rd Edition. Academic Press, Amsterdam, the Netherlands. https://doi.org/10.1016/C2010-0-65874-3

Rajh B, Yin CG, Samec N, et al., 2018. Advanced CFD modelling of air and recycled flue gas staging in a waste wood-fired grate boiler for higher combustion efficiency and greater environmental benefits. *Journal of Environmental Management*, 218:200-208. https://doi.org/10.1016/j.jenvman.2018.04.030

Rao ZH, Zhao YM, Huang CL, et al., 2015. Recent developments in drying and dewatering for low rank coals. *Progress in Energy and Combustion Science*, 46:1-11. https://doi.org/10.1016/j.pecs.2014.09.001

Sefidari H, Razmjoo N, Strand M, 2014. An experimental study of combustion and emissions of two types of woody biomass in a 12-MW reciprocating-grate boiler. *Fuel*, 135:120-129. https://doi.org/10.1016/j.fuel.2014.06.051

Shan SQ, Zhou ZJ, 2019. Second law analysis of spectral radiative transfer and calculation in one-dimensional furnace cases. *Entropy*, 21(5):461. https://doi.org/10.3390/e21050461

Shan SQ, Zhou ZJ, Chen LP, et al., 2017. New weighted-sum-of-gray-gases model for typical pressurized oxy-fuel conditions. *International Journal of Energy Research*, 41(15):2576-2595. https://doi.org/10.1002/er.3838

Shan SQ, Qian B, Zhou ZJ, et al., 2018. New pressurized WSGG model and the effect of pressure on the radiation heat transfer of H_2O/CO_2 gas mixtures. *International Journal of Heat and Mass Transfer*, 121:999-1010. https://doi.org/10.1016/j.ijheatmasstransfer.2018.01.079

Shan SQ, Zhou ZJ, Cen KF, 2019. An innovative integrated system concept between oxy-fuel thermo-photovoltaic device and a Brayton-Rankine combined cycle and its preliminary thermodynamic analysis. *Energy Conversion and Management*, 180:1139-1152. https://doi.org/10.1016/j.enconman.2018.11.040

Stanley C, Mojiri A, Rosengarten G, 2016. Spectral light management for solar energy conversion systems. *Nanophotonics*, 5(1):161-179. https://doi.org/10.1515/nanoph-2016-0035

Turns SR, 2012. An Introduction to Combustion: Concepts and Applications, 3rd Edition. McGraw-Hill Higher Education, New York, USA.

Tyagi VV, Kaushik SC, Tyagi SK, 2012. Advancement in solar photovoltaic/thermal (PV/T) hybrid collector technology. *Renewable and Sustainable Energy Reviews*, 16(3):1383-1398. https://doi.org/10.1016/j.rser.2011.12.013

Vodička M, Haugen NE, Gruber A, et al., 2018. NO_x formation in oxy-fuel combustion of lignite in a bubbling fluidized bed–modelling and experimental verification. *International Journal of Greenhouse Gas Control*, 76:208-214. https://doi.org/10.1016/j.ijggc.2018.07.007

Wang YL, Ma ZY, You HH, et al., 2018. Development of a NO_x emission model with seven optimized input parameters for a coal-fired boiler. *Journal of Zhejiang University-SCIENCE A (Applied Physics & Engineering)*, 19(4):315-328. https://doi.org/10.1631/jzus.A1600787

Xu J, Sun R, Ismail TM, et al., 2018. Nitrogen/NO conversion

characteristics of coal chars prepared using different pyrolysis procedures under combustion conditions. *Fuel*, 211:484-491.
https://doi.org/10.1016/j.fuel.2017.08.078

Yin CG, Yan JY, 2016. Oxy-fuel combustion of pulverized fuels: combustion fundamentals and modeling. *Applied Energy*, 162:742-762.
https://doi.org/10.1016/j.apenergy.2015.10.149

Yörük CR, Meriste T, Sener S, et al., 2018. Thermogravimetric analysis and process simulation of oxy-fuel combustion of blended fuels including oil shale, semicoke, and biomass. *International Journal of Energy Research*, 42(6):2213-2224.
https://doi.org/10.1002/er.4011

Zhang ZZ, Zhu MM, Li JB, et al., 2018. Experimental study of ignition and combustion characteristics of single particles of Zhundong lignite. *Energy & Fuels*, 32(4):4221-4226.
https://doi.org/10.1021/acs.energyfuels.7b03145

Zhou H, Li Y, Tang Q, et al., 2017. Combining flame monitoring techniques and support vector machine for the online identification of coal blends. *Journal of Zhejiang University-SCIENCE A (Applied Physics & Engineering)*, 18(9):677-689.
https://doi.org/10.1631/jzus.A1600454

Zhou ZJ, Hu X, You Z, et al., 2013. Oxy-fuel combustion characteristics and kinetic parameters of lignite coal from thermo-gravimetric data. *Thermochimica Acta*, 553:54-59.
https://doi.org/10.1016/j.tca.2012.11.030

Zhou ZJ, Ding L, Wu L, et al., 2014. Comparison of structure and gasification reactivity of rapid pyrolysis chars of coal water slurries and parent coals. *Energy Technology*, 2(3):284-291.
https://doi.org/10.1002/ente.201300172

Zhou ZJ, Guo LZ, Chen LP, et al., 2018. Study of pyrolysis of brown coal and gasification of coal-water slurry using the ReaxFF reactive force field. *International Journal of Energy Research*, 42(7):2465-2480.
https://doi.org/10.1002/er.4029

中文概要

题　目： 一维固定床煤粉富氧燃烧的辐射能流特性与模型分析

目　的： 1. 从辐射能利用角度出发，探究一维固定床煤粉富氧燃烧的辐射能流特性，为固体燃料燃烧能量分质分级转化应用提供参考；2. 对比研究半经验模型与人工神经网络模型这两种建模方法，为人工神经网络模型在后续研究中的应用提供参考。

创新点： 1. 提出燃烧光热能量分级转化的概念，为燃烧光热能量分质分级转化系统提供研究基础；2. 从辐射能量利用的角度研究煤粉燃烧的辐射能流特性；3. 不局限于实验报告，基于实验数据探究 2 种建模方法，揭示神经网络模型的优势。

方　法： 1. 在一维管式炉反应器上进行实验，探究不同燃烧条件下煤粉富氧燃烧的辐射能流特征；2. 基于辐射传热理论，通过半经验模型描述煤粉在固定床中燃烧的辐射能流；3. 训练神经网络模型来描述实验结果，通过对比 2 种方法来揭示神经网络模型在预测结果方面的优势。

结　论： 1. 固定床煤燃烧过程中的挥发分及煤烟会降低辐射能；可利用低挥发分燃料以及增大氧浓度来提高火焰辐射能比例。2. 较高的燃烧温度是提升燃烧辐射能比例最重要的因素；实践中可以通过采用高热值燃料以及烟气回热等方法来提高燃烧温度。3. 多联产半焦燃烧辐射能比例高于原煤；可通过煤热解多联产技术与半焦燃烧光热能量分级利用相结合的方式构成新的煤炭高效清洁利用系统。4. 人工神经网络不但可以对实验结果进行建模，还能够很好地预测未知工况结果，因此值得在更多的后续研究中使用。

关键词： 辐射能流；固定床；富氧燃烧；人工神经网络；能量分质分级转化